SEISMIC POUNDING ANALYSIS OF NEIGHBORING BUILDINGS UNDER LONG-PERIOD GROUND MOTION

Daigoro ISOBE, *Department of Engineering Mechanics and Energy, University of Tsukuba*
1-1-1 Tennodai, Tsukuba-shi,Ibaraki 305-8573, JAPAN
Email: isobe@kz.tsukuba.ac.jp
Tokiharu OHTA, *Collaborative Research Center, Ashikaga Institute of Technology, JAPAN*
Tomohiro INOUE, *Science Programs Division, Japan Broadcasting Corporation, JAPAN*
Fujio MATSUEDA, *Kyoryo Consultants Ltd. , JAPAN*

***Keywords*:** seismic pounding, long-period ground motion, collapse analysis, FEM, ASI-Gauss technique

SUMMARY

Seismic pounding phenomena, namely the collision of neighboring buildings under long-period ground motion, are becoming a major issue in Japan. We focused on a specific apartment house called Nuevo Leon buildings in Tlatelolco district of Mexico City, with three same type buildings consecutively built with very narrow expansion joints in between. Two out of the three collapsed totally in 1985 Mexican Earthquake. Using a finite element code based upon the adaptively shifted integration (ASI)-Gauss technique, a seismic pounding analysis is carried out on a simulated model of Nuevo Leon buildings to realize the impact and collapse behavior of the buildings built in the vicinity of each other. The numerical code used in the analysis provides higher computational efficiency than the conventional code in this kind of problems, and enables us to cope with dynamic behavior with strong nonlinearities including phenomena such as member fracture and elemental contact. Contact release and re-contact algorithms are also developed and implemented in the code to realize complex behaviors of structural members during seismic pounding and collapse sequence. According to the numerical results, collision of buildings may well be generated by the difference of natural periods between the neighboring buildings. This was actually detected in the same type of buildings due to the damages caused by the past earthquakes. By setting the natural period of the north building to be 25 % longer than the others, the ground motion with relatively long period of 2 s first caused the collision between the north and the middle buildings. This eventually led the middle to collapse, followed by the destruction of the north.

1. INTRODUCTION

Seismic pounding phenomena, namely the collision of neighboring buildings under long-period ground motion, are becoming a major issue in Japan. In 1985 Mexican Earthquake, many apartment houses collapsed due to long-period ground motion. It was crucial especially in Mexico City, which was about 400 km away from the epicenter (see Fig. 1). We focused on a specific apartment house called Nuevo Leon buildings in Tlatelolco district of Mexico City, with three same type 14-story buildings consecutively built with very narrow gaps of 10 cm in between (see Fig. 2). Two out of the three collapsed totally in the great earthquake (see Fig. 3).

We carried out a seismic pounding analysis on a simulated model of Nuevo Leon buildings to realize the impact and collapse behavior of the buildings built in the vicinity of each other. We used a finite element code based upon the adaptively shifted integration (ASI)-Gauss technique [Lynn and Isobe, 2007] which provides higher computational efficiency than the conventional code in this kind of problems, and enables us to cope with dynamic

Figure 1 Epicenter of the 1985 Mexican earthquake

Figure 2 Nuevo Leon buildings before the earthquake

Figure 3 Collapse of the Nuevo Leon buildings (south building at the far side, picture by Marco Antonio Cruz)

behavior with strong nonlinearities including phenomena such as member fracture and elemental contact. Contact release and re-contact algorithms are also developed and implemented in the code to realize complex behaviors of structural members during seismic pounding and collapse sequence. In the analysis, we set the natural period of one building out of the three to be 25% longer than the others, as the difference of natural periods was actually observed in the same type buildings caused by the damage that remained after past earthquakes.

2. NUMERICAL METHODS

General concept of the ASI-Gauss technique in comparison with the earlier version of the technique, the ASI technique [Toi and Isobe, 1993] is explained in this section. Moreover, algorithms considering member fracture and elemental contact, and incremental equation of motion for excitation at fixed points, are described.

2.1 ASI-Gauss Technique

Figure 4 shows a linear Timoshenko beam element and its physical equivalence to the rigid bodies-spring model (RBSM). As shown in the figure, the relationship between the locations of the numerical

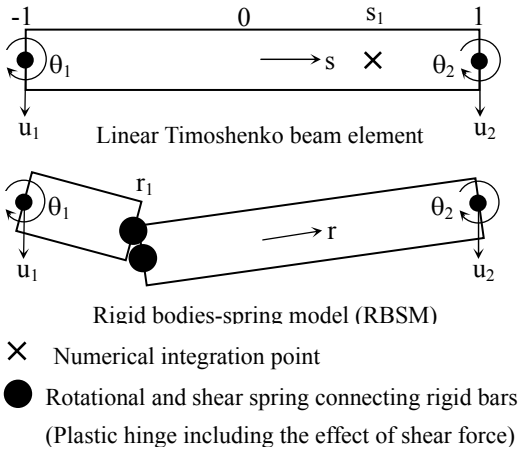

Figure 4 Linear Timoshenko beam element and its physical equivalent

integration point and the stress evaluation point where a plastic hinge is actually formed is expressed as [Toi, 1991]

$$r = -s \tag{1}$$

In the above equation, s is the location of the numerical integration point, and r the location where stresses and strains are actually evaluated. We refer to r as the stress evaluation point later in this paper. s and r are nondimensional quantities, which take values between -1 and 1.

In both the ASI and ASI-Gauss techniques, the numerical integration point is shifted adaptively when a fully plastic section is formed within an element to form a plastic hinge at exactly that section. When the plastic hinge is determined to be unloaded, the corresponding numerical integration point is shifted back to its normal position. Here the normal position means the location where the numerical integration point is placed when the element acts elastically. By doing so, the plastic behavior of the element is simulated appropriately, and the converged solution is achieved with only a small number of elements per member. However, in the ASI technique, the numerical integration point is placed at the midpoint of the linear Timoshenko beam element, which is considered to be optimal for one-point integration, when the entire region of the element behaves elastically. When the number of elements per member is very small, solutions in the elastic range are not accurate enough because one-point integration is used to evaluate the low-order displacement function of the beam element.

The main difference between the ASI and ASI-Gauss techniques lies in the normal position of the numerical integration point. In the ASI-Gauss technique, two consecutive elements forming a member are considered as a subset, and the numerical integration points of an elastically deformed member are placed such that the stress evaluation points coincide with the Gaussian integration points of the member. This means that stresses and strains are evaluated at the Gaussian integration points of elastically deformed members. Gaussian integration points are optimal for two-point integration, and the accuracy of bending deformation is mathematically guaranteed [Press et al, 1992]. In this way, the ASI-Gauss technique takes advantage of two-point integration while using one-point integration in actual calculations.

Figure 5 shows the locations of the numerical integrations points of elastically deformed elements in the ASI and ASI-Gauss techniques. The elemental stiffness matrix, generalized strain and sectional force increment vectors in the elastic range for the ASI technique are given by Eqs. (2) and those for the ASI-Gauss technique by Eqs. (3).

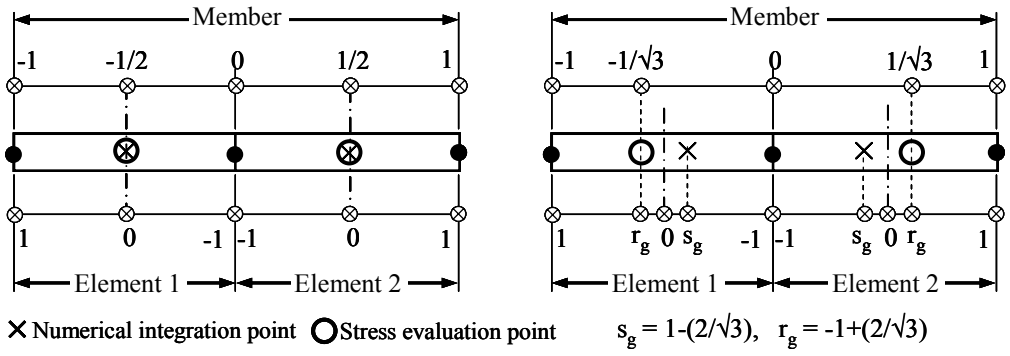

(a) ASI technique (b) ASI-Gauss technique

Figure 5 Locations of numerical integration and stress evaluation points in elastic range

$$[K]=L[B(0)]^T[D(0)][B(0)] \quad (2a)$$

$$\{\Delta\varepsilon(0)\}=[B(0)]\{\Delta u\} \quad (2b)$$

$$\{\Delta\sigma(0)\}=[D(0)]\{\Delta\varepsilon(0)\} \quad (2c)$$

$$[K]=L[B(s_g)]^T[D(r_g)][B(s_g)] \quad (3a)$$

$$\{\Delta\varepsilon(r_g)\}=[B(s_g)]\{\Delta u\} \quad (3b)$$

$$\{\Delta\sigma(r_g)\}=[D(r_g)]\{\Delta\varepsilon(r_g)\} \quad (3c)$$

$$s_g = 1-\frac{2}{\sqrt{3}}, \qquad r_g = -1+\frac{2}{\sqrt{3}} \quad (3d)$$

Here, $\{\Delta\varepsilon\}$, $\{\Delta\sigma\}$ and $\{\Delta u\}$ are the generalized strain increment vector, generalized stress (sectional force) increment vector and nodal displacement increment vector, respectively. $[B]$ is the generalized strain-nodal displacement matrix, $[D]$ is the stress-strain matrix, and L is the length of the element.

The plastic potential used in this study is expressed by

$$f=\left(\frac{M_x}{M_{x0}}\right)^2+\left(\frac{M_y}{M_{y0}}\right)^2+\left(\frac{N}{N_0}\right)^2-1=f_y-1=0 \quad (4)$$

Here, f_y is the yield function, and M_x, M_y and N are the bending moments around the x- and y- axes and axial force, respectively. Those with the subscript 0 are values that result in a fully plastic section in an element when they act on a cross section independently. The effect of torsion and shear force is neglected in the yield function.

2.2 Member Fracture and Contact Algorithm

A plastic hinge is likely to occur before it develops to a member fracture, and the plastic hinge is expressed by shifting the numerical integration point to the opposite end of the fully-plastic section. Accordingly, the numerical integration point of the adjacent element forming the same member is shifted back to its midpoint where it is appropriate for one-point integration. Figure 6 shows the locations of numerical integration points for each stage in the ASI-Gauss technique.

Member fracture is determined, in this study, by means of curvatures, shear strains and axial tensile strain occurred in the elements as shown in the following equation.

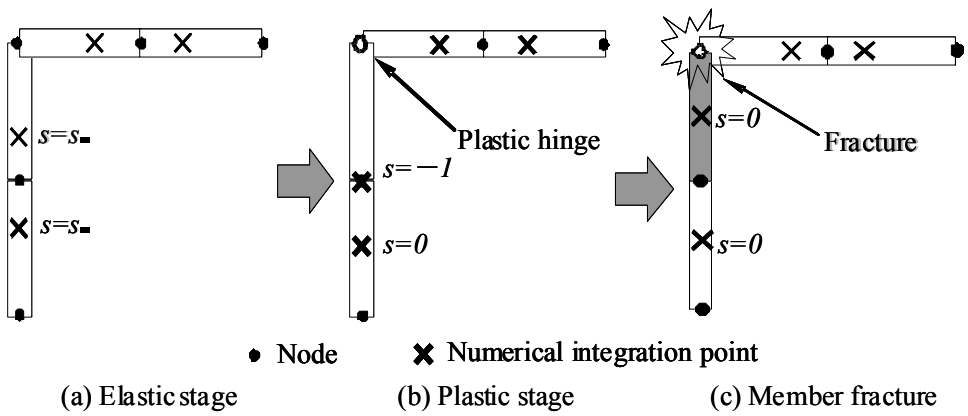

(a) Elastic stage (b) Plastic stage (c) Member fracture

Figure 6 Locations of numerical integration points in each stage

$$\left|\frac{\kappa_x}{\kappa_{x0}}\right| - 1 \geq 0 \quad \text{or} \quad \left|\frac{\kappa_y}{\kappa_{y0}}\right| - 1 \geq 0 \quad \text{or} \quad \left|\frac{\gamma_{xz}}{\gamma_{xz0}}\right| - 1 \geq 0$$

$$\text{or} \quad \left|\frac{\gamma_{yz}}{\gamma_{yz0}}\right| - 1 \geq 0 \quad \text{or} \quad \frac{\epsilon_z}{\epsilon_{z0}} - 1 \geq 0 \tag{5}$$

where κ_x, κ_y, γ_{xz}, γ_{yz}, ε_z, κ_{x0}, κ_{y0}, γ_{xz0}, γ_{yz0} and ε_{z0} are the curvatures around the x- and y-axes, the shear strains for the x- and y-axes, the axial tensile strain and the critical values for these strains, respectively. We fixed the critical values using the information from actual experimental data [Hirashima et al, 2007]. Contact determination is done by examining the geometrical locations of the elements and once two elements are determined to be in contact, they are bound with a total of four gap elements between the nodes [Lynn and Isobe, 2007]. The sectional forces are delivered through these gap elements to the connecting elements. To express contact release, the gap elements are automatically eliminated at the time when the mean value of the deformation of gap elements is reduced to a specified ratio.

2.3 Incremental Equation of Motion

The dynamic equilibrium equation at time step t=t can be formulated as

$$[M]\{\ddot{u}\}_t = \{E\}_t - \{F\}_t \tag{6}$$

where $[M]$, $\{\ddot{u}\}_t$, $\{E\}_t$ and $\{F\}_t$ are the mass matrix, acceleration vector, nodal external force vector and internal force vector at time step t=t, respectively.

The following equation is substituted into Eq. (6) at t=t+1 in the implicit code:

$$\{F\}_{t+1} = \{F\}_t + [K]\{\Delta u\} \tag{7}$$

Then the following incremental stiffness equation is evaluated:

$$[M]\{\ddot{u}\}_{t+1} + [K]\{\Delta u\} = \{E\}_{t+1} - \{F\}_t \tag{8}$$

where $[K]$ is a stiffness matrix at time step t=t. By neglecting residual forces, an implicit code is obtained by evaluating the following incremental equation of motion:

$$[M]\{\Delta\ddot{u}\} + [K]\{\Delta u\} = 0 \tag{9}$$

Consequently, the incremental equation of motion for a structure under excitation at fixed points, which is used in this paper, yields to:

$$[M_1]\{\Delta\ddot{u}\} + [M_2]\{\Delta\ddot{u}_b\} + [K_1]\{\Delta u\} + [K_2]\{\Delta u_b\} = 0 \tag{10}$$

The subscript '1' indicates the coupled terms between free nodal points, '2' indicates the coupled terms between free nodal and fixed nodal points, and 'b' indicates the components at fixed nodal points. Vectors $\{\Delta\ddot{u}\}$ and $\{\Delta u\}$ are the nodal acceleration increment and the nodal displacement increment, respectively.

Under the assumption that the displacements at free nodal points are estimated by adding quasi-static displacement increments $\{\Delta u_s\}$ and dynamic displacement increments $\{\Delta u_d\}$, the displacements at free nodal points are given as

$$\{\Delta u\} = \{\Delta u_s\} + \{\Delta u_d\} \tag{11}$$

$\{\Delta u_s\}$ is evaluated, by neglecting inertia force, as follows:

$$\{\Delta u_s\} = -[K_1]^{-1}[K_2]\{\Delta u_b\} \tag{12}$$

Substituting Eq. (11) and Eq. (12) into Eq. (10), the following equation is obtained:

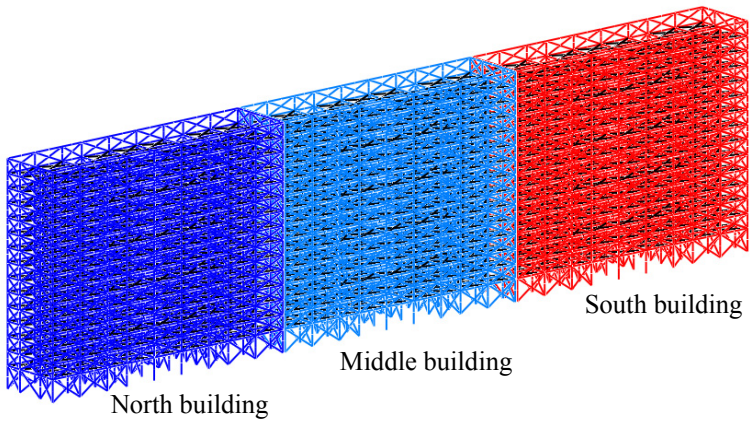

Figure 7 Numerical models of three connected buildings

Table 1 Sectional properties of the structural members

	Columns (1~5 Fl.)	Columns (6~10 Fl.)	Columns (11~12 Fl.)
Section (mm)	□330×330×10	□280×280×9	□230×230×7
	Beams	Floor slabs	
Section (mm)	H292×730.0×16.2×11.6	□230×230×7	

Table 2 Natural period of each building model

	NS	EW
North	1.5 s	1.72 s
Middle	1.2 s	1.65 s
South	1.2 s	1.65 s

Table 3 Natural period of Chihuanua, the same type building

	NS			EW		
Building No.	1	2	3	1	2	3
Natural period (s)	1.39	1.11	1.13	1.94	1.63	1.77
Ratio of period to No.2 building	1.25	1.0	1.02	1.19	1.0	1.09

$$[M_1]\{\Delta\ddot{u}_d\} + [K_1]\{\Delta u_d\} = ([M_1][K_1]^{-1}[K_2] - [M_2])\{\Delta\ddot{u}_b\} \quad (13)$$

In this scheme, equivalent forces are calculated by substituting nodal acceleration increments at fixed points into the right side of the above equation.

3. SEISMIC POUNDING ANALYSIS OF NEIGHBORING BUILDINGS

A seismic pounding analysis is carried out, using the numerical code shown above, on neighboring buildings to investigate the effects of collisions between them during a long-period ground motion. We modeled a specific apartment house, as shown in Fig. 7, with three same type 14-story buildings consecutively built with very narrow gaps of 10 cm in between. The model is 42.02 m high and 12.4 m wide, with a total length of 160 m. By referring to the design guideline of Mexico in 1985, the base shear coefficient is set to 0.06 and the axial force ratio on the 1st floor to 0.5. The dead load for each floor is set to 4.0 kN/m^2 and the damping ratio to 5 %. The Nuevo Leon buildings are originally built with reinforced concrete (RC) members; however, the model constructed in this study is intentionally made with steel members to easily verify the influence of structural parameters such as member fracture strains. Critical curvatures for fracture are set to 3.333×10^{-4}, critical shear strains to 3.380×10^{-4} and critical axial tensile strain to 0.17, respectively. The critical shear strains are lowered than those of steel members to consider the characteristics of RC beams. The sectional properties of the structural members are shown in Table 1. The time increment is set to 1 ms, and the calculation is done for a total of 90,000 steps. The analysis takes approximately 4 days with a personal computer (CPU: 2.93 GHz Xeon).

In this case, we set the natural period of the north building model to be 25% longer than the others, as shown in Table 2, by lowering the structural strengths of the columns. The difference of natural periods was actually observed in the same type buildings built near the site (see Table 3), caused by the damage that remained after past earthquakes [Ciudad de Mexico,

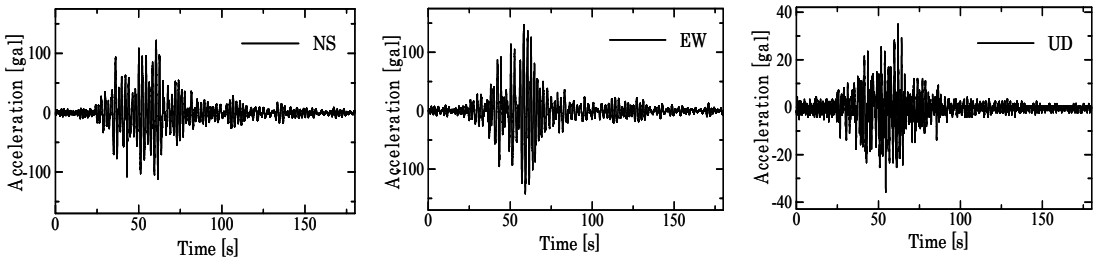

Figure 8 Ground acceleration (SCT wave)

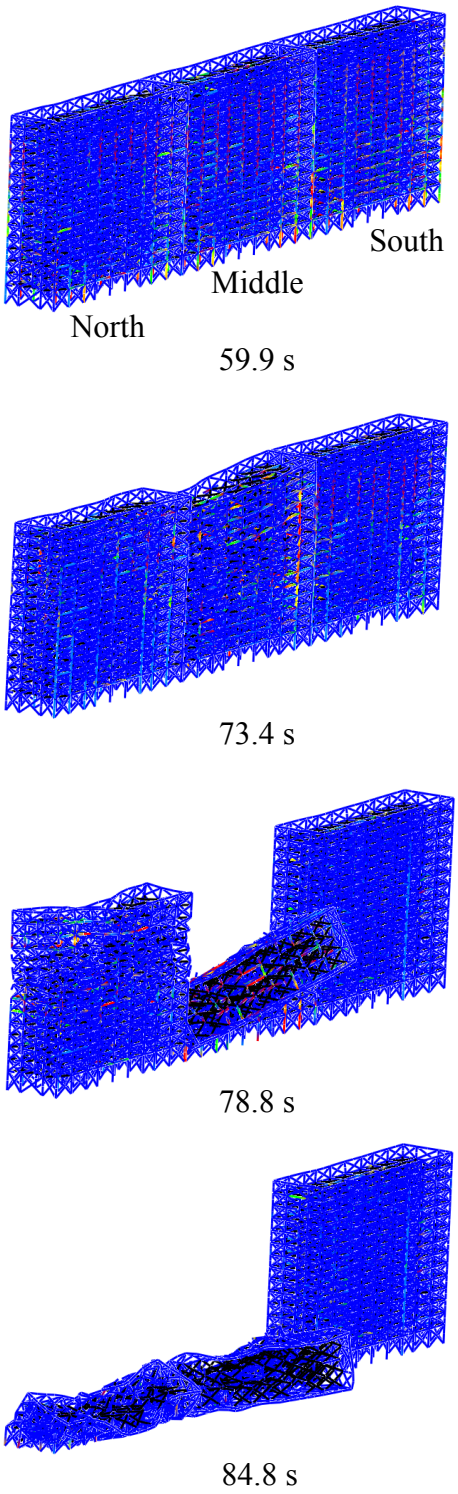

Figure 9 Collapse behaviors of neighboring buildings under long-period ground motion

1986]. EW, NS and UD components of SCT seismic wave shown in Fig. 8 are subjected to the fixed points on the ground floor. The intensity period of the seismic wave was about 2 s due to the reclaimed soft soil of Mexico valley. According to the numerical results such as in Fig. 9, the collision of buildings may be generated by the difference of natural periods between neighboring buildings. The north building with a longer natural period first collides with the middle, consequently changing the natural period of the middle, which ends up generating other collisions between the south and the middle. The middle building first initiates collapse due to continuous collisions given from both sides, around 73 s from the start of seismic activity. Although the north building collapses a few seconds after the middle, the south building withstands the collisions and resists to collapse.

4. CONCLUSIONS

The numerical result shown in this paper clarifies the possibility that the long-period ground motion might cause extra damage on high-rise architectures due to inter-building collisions if the distances between them are not sufficiently secured. Extra cautions might be needed if the natural periods of the neighboring buildings are different, which can be easily fulfilled, for example, by the difference of their heights.

5. REFERENCES

Ciudad de Mexico. (1986), Programa de Reconstruccion Nonoalco/Tlatelolco, Tercera Reunion de la Comision Tecnica Asesora (the Third Meeting of the Technical Commission Advises).

Hirashima, T., Hamada, N., Ozaki, F., Ave, T. and Uesugi, H. (2007), "Experimental Study on Shear Deformation Behavior of High Strength Bolts at Elevated Temperature", *Journal of Structural and Construction Engineering*, Vol.621, pp.175-180, in Japanese.

Lynn, K.M. and Isobe, D. (2007), "Finite Element Code for Impact Collapse Problems of Framed Structures", *International Journal for Numerical Methods in Engineering*, Vol.69, No.12, pp. 2538-2563.

Press, W.H., Teukolsky, S.A., Vetterling, W.T. and Flannery, B.P. (1992), Numerical Recipes in FORTRAN: The Art of Scientific Computing, New York: Cambridge University Press.

Toi, Y. (1991), "Shifted Integration Technique in One-Dimensional Plastic Collapse Analysis Using Linear and Cubic Finite Elements", *International Journal for Numerical Methods in Engineering*, Vol.31, pp.1537-1552.

Toi, Y and Isobe, D. (1993), "Adaptively Shifted Integration Technique for Finite Element Collapse Analysis of Framed Structures", *International Journal for Numerical Methods in Engineering*, Vol.36, pp.2323-2339.